JVI Journals.ASM.org

The Tobamovirus *Turnip Vein Clearing Virus* 30-Kilodalton Movement Protein Localizes to Novel Nuclear Filaments To Enhance Virus Infection

Amit Levy, Judy Y. Zheng, Sondra G. Lazarowitz

Cornell University, Department of Plant Pathology and Plant-Microbe Biology, Ithaca, New York, USA

Plant viruses overcome the barrier of the plant cell wall by encoding cell-to-cell movement proteins (MPs), which direct newly replicated viral genomes to, and across, the wall. The paradigm for how a single MP regulates and coordinates these activities is the *Tobacco mosaic virus* (TMV) 30-kDa protein (MP^{TMV}). Detailed studies demonstrate that TMV multiplies exclusively in the cytoplasm and have documented associations of MP^{TMV} with endoplasmic reticulum (ER) membrane, microtubules, and plasmodesmata throughout the course of infection. As TMV poorly infects *Arabidopsis thaliana*, *Turnip vein clearing virus* (TVCV) is the tobamovirus of choice for studies in this model plant. A key problem, which has contributed to confusion in the field, is the unproven assumption that the TVCV and TMV life cycles are identical. We engineered an infectious TVCV replicon that expressed a functional fluorescence-tagged MP^{TVCV} and report here the unexpected discovery that MP^{TVCV}, beyond localizing to ER membrane and plasmodesmata, targeted to the nucleus in a nuclear localization signal (NLS)-dependent manner, where it localized to novel F-actin-containing filaments that associated with chromatin. The MP^{TVCV} NLS appeared to be conserved in the subgroup 3 tobamoviruses, and our mutational analyses showed that nuclear localization of MP^{TVCV} was necessary for efficient TVCV cell-to-cell movement and systemic infection in *Nicotiana benthamiana* and *Arabidopsis thaliana*. Our studies identify a novel nuclear stage in TVCV infection and suggest that nuclear MP encoded by TVCV and other subgroup 3 tobamoviruses interacts with F-actin and chromatin to modulate host defenses or cellular physiology to favor virus movement and infection.

The plant cell wall is a barrier to virus exit from and entry into cells. Thus, successful infection requires that plant viruses encode movement proteins to transport the viral genome locally cell to cell within a leaf and on into the vascular system, through which the virus will systemically invade the plant. Cell-to-cell movement occurs via a common pathway: plant viruses exploit plasmodesmata (PD), membranous transwall channels that connect adjacent plant cells. Cell-to-cell movement proteins (hereafter designated MP, with the specific virus indicated) alter PD permeability and thereby enable transport of the viral genome into adjacent cells (1). Beyond this essential role in intercellular trafficking, movement proteins act to coordinate replication of the viral genome with its directed transport to PD. Depending on their replication strategy, plant viruses may encode additional movement proteins (hereafter referred to by their virus-specific names) to bind the viral genome and coordinate intracellular trafficking events with the cell-to-cell MP. However, many plant viruses utilize a single MP to coordinate intracellular and intercellular trafficking events, as typified by the 30-kDa MP^{TMV} encoded by the tobamovirus *Tobacco mosaic virus* (TMV) (2, 3). In general, virion assembly is not essential for cell-to-cell movement. Indeed, for TMV and most other plant viruses, viral coat protein (CP) is not required for intercellular trafficking, although it is essential for systemic spread (2).

Much of our understanding of movement protein function is based on pioneering studies of TMV, a positive-sense RNA (+RNA) virus that, like most RNA viruses, multiplies entirely within the cytoplasm of the infected cell. Upon virion uncoating, the TMV +RNA genome is first translated into the viral replicase, which initiates an early phase of viral RNA replication at sites associated with endoplasmic reticulum (ER)-derived membranes. This includes synthesis of two distinct subgenomic RNAs that encode MP^{TMV} and CP (4). As the viral life cycle progresses, TMV genomes associate with additional ER sites to amplify replication and eventually traffic to and through PD. MP^{TMV} shares two hallmark features with other +RNA virus so-called "30K-like" MPs, namely, the ability to bind nucleic acids and to alter the gating properties of PD (5), which suggests a potential role in coordinating these intracellular trafficking events with cell-to-cell movement. Such a key role for MP^{TMV} in distributing viral RNA within infected cells is indicated by studies employing an infectious clone of TMV that encodes a functional fusion of MP^{TMV} to the green fluorescent protein (GFP). This TMV replicon has been used in confocal microscopy studies to examine the associations of MP^{TMV} with cellular components during the time course of virus infection in individual expanding infection sites, visualized as fluorescent foci on inoculated leaves of *Nicotiana benthamiana*, which is a permissive host (6). Early (leading edge of foci) and throughout the infection site, MP^{TMV}-GFP localizes to discrete punctae at the cell periphery, which appear to mark the location of PD (6). Early in infection, MP^{TMV}-GFP is also on motile cytosolic vesicles and accumulates at sites derived from ER membranes. The latter appear to be sites of viral replication and protein synthesis as they contain replicase, viral RNA, and CP (6–8). These replication sites

Received 8 December 2012 **Accepted** 21 March 2013
Published ahead of print 27 March 2013
Address correspondence to Sondra G. Lazarowitz, SGL5@cornell.edu.
Supplemental material for this article may be found at http://dx.doi.org/10.1128/JVI.03390-12.

doi:10.1128/JVI.03390-12

enlarge as infection progresses, during which the reticulate ER network collapses. At late times during infection (center of infection sites), MP^{TMV}-GFP appears to redistribute from replication sites to microtubules and is then degraded, at which point MP^{TMV}-GFP is seen only in small punctae at the periphery (PD) (6). This last finding and other studies (9–12) have led to the suggestion that microtubules direct MP^{TMV} to be degraded via proteasomes. However, the role of microtubules in TMV infection remains controversial (1, 12).

Turnip vein clearing virus (TVCV) is in *Tobamovirus* subgroup 3, which also includes *Ribgrass mosaic virus* (RMV) and *Youcai mosaic virus* (YoMV, reported to be the same as *Oilseed rape mosaic virus* [ORMV]) (13). In contrast to subgroup 1, which includes TMV and other tobamoviruses isolated from solanaceous plants, and also the orchid-infecting *Odontoglossum ringspot virus* (ORV) (14), subgroup 3 viruses were isolated from the Brassicaceae family (formerly called crucifers) and can all infect the model plant *Arabidopsis thaliana*. In contrast to TMV, TVCV efficiently infects the *Arabidopsis* Col-0 ecotype and has become the model tobamovirus for virus-host interaction studies that take advantage of the genetic, genomic, and molecular resources afforded by this model plant. It has generally been assumed that the TVCV life cycle, including MP^{TVCV} distribution during infection, follows the same stages as that of TMV, but this has not been proven. Indeed, host factors identified in *Arabidopsis* using TVCV are often studied in the context of TMV infection and interactions in *N. benthamiana*, in which transient assays and cellular studies can be easier to do.

In order to realize the full potential of TVCV for investigating virus-host interactions and cell-to-cell transport in *Arabidopsis*, we engineered a TVCV replicon that encodes a functional form of MP^{TVCV} fused to GFP or red fluorescent protein (RFP) and used these infectious clones to investigate the subcellular localization of MP^{TVCV} during the time course of TVCV infection in *Arabidopsis* Col-0 and *N. benthamiana*, both permissive hosts. As reported here, we unexpectedly discovered a nuclear stage in TVCV infection. Similarly to TMV, we found that MP^{TVCV} localized to PD and what appear to be ER-derived replication sites during the time course of virus infection in expanding infection sites. However, in striking contrast to TMV, we observed that MP^{TVCV} did not associate with microtubules but did accumulate in what appeared to be novel F-actin-containing nuclear filaments. We further identified a nuclear localization signal (NLS) in MP^{TVCV} that is conserved in the subgroup 3 tobamoviruses. We showed, through mutational analyses, that this NLS both was required for the nuclear localization of MP^{TVCV} and was necessary for efficient TVCV cell-to-cell spread and systemic infection in both *N. benthamiana* and *Arabidopsis*. Our studies identify a novel nuclear stage in TVCV infection and suggest that nuclear targeting of MP encoded by TVCV and potentially other subgroup 3 tobamoviruses may play a role in modulating host defense or cellular physiology to favor virus movement and infection.

MATERIALS AND METHODS

Generation of fusion proteins and TVCV replicons. We used Gateway technology to construct MP^{TVCV} C-terminal fusions to GFP (MP^{TVCV}-GFP) or monomeric RFP (MP^{TVCV}-RFP). We amplified the *MP*^{TVCV} coding sequence located between HindIII and NsiI sites in pBluescript KS(+)-MP^{TVCV} using PCR and cloned it into the donor vector pDONR207 and then into the pSITE 2NB or pSITE 4NB destination vector (15) to generate pSITE2NB::MP^{TVCV}-GFP and pSITE4NB::MP^{TVCV}-RFP, respectively. To construct the viral replicon clones pTVCV::MP-GFP and pTVCV::MP-RFP, the C-terminal GFP/RFP-fused coding sequence of MP^{TVCV} starting at nucleotide (nt) 580 (an internal EcoRI site) was PCR amplified from each of these vectors to add a 3′-terminal PpuMI site following the *GFP* or *RFP* stop codon, and each fragment was then cloned between the EcoRI and PpuMI sites of pTVCV50, which contains the infectious TVCV full-length genomic cDNA clone under the control of the SP6 promoter (16). The resulting TVCV replicons TVCV::MP-GFP and TVCV::MP-RFP each expressed MP^{TVCV} (the GFP or RFP fusion) from the endogenous *MP* promoter but were deleted for the *CP* gene, which overlaps the 3′ end of the *MP* coding region (14).

To generate the NLS virus [$TVCV^{MP(K210A/K212A)}$] and replicon (TVCV::$MP^{K210A/K212A}$-GFP) mutants, we used PCR mutagenesis (17) to change nt 628 to 630 from AAG to GCT and nt 634 to 635 from AA to GC in the MP^{TVCV} coding sequence in pTVCV50 and pTVCV::MP-GFP, respectively, thereby substituting Ala residues for Lys at positions 210 and 212 in MP^{TVCV}. In brief, each plasmid was amplified with *Pfu* ultra-high-fidelity DNA polymerase (Agilent, CA) using the complementary primers 5′-GCGGTTGACAATTTCAGGGCTAGGGCAAAGAAGGTTGAAGAAAGGGATG-3′ and 5′-CATCCCTTTCTTCAACCTTCTTTGCCCTAGCCCTGAAATTGTCAACCGC-3′, followed by template digestion with DpnI. To construct the N-terminal glutathione *S*-transferase (GST) fusions GST-MP^{TVCV} and GST-$MP^{TVCV(K210A/K212A)}$, the coding sequences for each were amplified from pTVCV50 and $pTVCV^{MP(K210A/K212A)}$, respectively, using primers that contain 5′ BamHI and 3′ XhoI restriction sites, and each was then cloned between the BamHI and XhoI sites in pGEX-5X-1 (GE Healthcare Biosciences, Piscataway, NJ). To generate the TagRFP-UtrCH fusion, we PCR amplified the calponin homology domain of utrophin (18) from pCS2(+)-GFP-UtrCH (Addgene, Cambridge, MA). This was cloned into pDONR207 and then into the pSITEII 6C1 destination vector (19) to generate pSITEII6C1::TagRFP-UtrCH.

All constructs were confirmed by DNA sequence analysis performed on an Applied Biosystems automated 3730 DNA analyzer at the Cornell University Life Sciences Core DNA Sequencing Lab.

Plant infectivity and transient expression assays. For transient expression studies using agroinfiltration, *N. benthamiana* plants were grown and maintained under greenhouse conditions of 22°C with 16-h supplemental lighting. For local infection site and infectivity assays, *N. benthamiana* plants were grown and maintained in growth chambers at 25°C under long-day (16-h-light/8-h-dark) conditions. *Arabidopsis* ecotype Col-0 plants were grown in growth rooms or chambers at 22°C. These plants were initially grown under short-day (8-h-light/16-h-dark) conditions for local infection site studies or under long-day (16-h-light/8-h-dark) cycle for infectivity studies. Following inoculations, Col-0 plants were maintained under long-day conditions.

For nuclear localization studies of MP^{TVCV}, pSITE2NB::MP^{TVCV}-GFP or pSITE2NB::$MP^{TVCV(K210A/K212A)}$-GFP was agroinfiltrated into 4- to 5-week transgenic *N. benthamiana* lines that expressed either histone 2B-RFP to label chromatin (19) or fibrillarin-RFP to label nucleoli (19), using cultures of *Agrobacterium tumefaciens* GV2260 at an optical density at 600 nm (OD_{600}) of 0.05 as previously described (20), and plants were imaged at 40 h postinfiltration (p.i.). To coexpress MP^{TVCV}-GFP and the actin probe TagRFP-UtrCH, GV2260 cultures at an OD_{600} of 0.01 for pSITE2NB::MP^{TVCV}-GFP and pSITEII6C1::TagRFP-UtrCH were mixed in equal volumes and coinfiltrated into wild-type (wt) *N. benthamiana*. Cell-to-cell movement of MP^{TVCV}-GFP and $MP^{TVCV\ (K210A/K212A)}$-GFP was assayed by transient expression in *N. benthamiana* leaf epidermal cells, as previously described (21). In brief, pSITE2NB::MP^{TVCV}-GFP or pSITE2NB::$MP^{TVCV(K210A/K212A)}$-GFP was agroinfiltrated into *N. benthamiana* leaves at an OD_{600} of 0.0005. To control for leaf variability, plasmid pairs were agroinfiltrated into different sectors on the same leaf for direct comparisons. We used confocal microscopy to count cells in

individual fluorescent foci at 40 to 44 h p.i. and analyzed the results by *t* test.

For local infection site studies, plants were inoculated with *in vitro*-synthesized infectious genomic +RNA transcripts. Plasmids pTVCV::MP^{TVCV}-GFP and pTVCV::MP^{TVCV}-RFP carrying the viral replicons TVCV::MP-GFP and TVCV::MP-RFP, respectively, were linearized with KpnI, and RNA was transcribed using the SP6 mMessage Machine kit (Life Technologies, Grand Island, NY). Leaves from 4- to 5-week-old wild-type (wt) *N. benthamiana* plants or transgenic lines that expressed compartment-specific markers (ER, GFP-HDEL [22]; actin cytoskeleton, talin-GFP [19]; chromatin, histone 2B-RFP [19]; microtubules, TUA-GFP [23]) were rub inoculated with the infectious +RNA transcripts using Celite (Sigma, St. Louis, MO) (16), and expanding fluorescent foci were imaged at 4 days p.i. by confocal microscopy. To directly compare the relative cell-to-cell spread of TVCV::MP-GFP and that of TVCV::MP$^{K210A/K212A}$-GFP, half of each leaf was inoculated with a standardized amount of +RNA for each replicon (20% of the +RNA produced by *in vitro* transcription of 1 μg DNA template) and the sizes of infection sites were scored at 5 days p.i. using a stereomicroscope and ImageJ software (http://rsbweb.nih.gov/ij/). *Arabidopsis* Col-0 plants were inoculated at the 12- to 14-leaf stage as described for *N. benthamiana* and imaged by confocal microscopy at 7 days p.i.

For infectivity assays, plants were inoculated with leaf extracts from *N. benthamiana* plants infected with wt p50TVCV or pTVCV$^{MP(K210A/K212A)}$. Systemically infected leaves were frozen and ground in 10 ml phosphate-buffered saline (PBS) and 0.1 g Celite per gram of leaf tissue, and extracts were clarified by centrifugation at 5,000 × *g* for 5 min prior to use. To quantify the relative amounts of virus in these extracts, CP intensities in 2, 3, 4, and 5 μl were determined by SDS-PAGE and, based on this, plants were rub inoculated with equivalent amounts of virus. To determine infectivity in *N. benthamiana*, 4- to 5-week-old plants were inoculated with virus-containing extract or mock inoculated with PBS, and systemic symptoms were scored daily after infection. To detect CP in systemically infected leaves, extracts from a leaf disc (1-cm diameter) punched from the third leaf from the top of infected plants were prepared and CP was detected by SDS-PAGE and Coomassie blue staining, as previously described (24). For infectivity assays in *Arabidopsis*, Col-0 plants at the 8-leaf stage were inoculated with appropriate amounts of virus-containing extracts or with PBS. Infectivity was determined based on the levels of viral CP in extracts of systemic leaves (0.5 g tissue/ml buffer), as determined by SDS-PAGE and Coomassie blue staining. Statistical analyses were done using JMPPro 0.0.2 software (SAS, Cary, NC). Local cell-to-cell spread was analyzed using a *t* test, and the Wilcoxon test was applied to infectivity assays.

Replication assays. Leaf mesophyll protoplasts were isolated from leaves of 4- to 5-week-old *N. benthamiana* plants and transfected with 2 μg of TVCV or TVCV::MP$^{(K210A/K212A)}$ +RNA transcripts, as previously described (21). Total RNA was isolated at 0 h, 4 h, and 20 h post-transfection using TRIzol (Life Technologies, Grand Island, NY), and following incubation with DNase I (Life Technologies, Grand Island, NY), reverse transcription was performed using Omniscript reverse transcriptase (Qiagen, Hilden, Germany) and the following primers: TVCV minus strand (−RNA), 5′-ATGAGGCCGTTGCCGAG-3′; 18S rRNA internal control, 5′-AGTCTGTCAATCCTTACTAT-3′. Semiquantitative reverse transcription-PCR (sqRT-PCR) analyses were performed as described previously (21), using primers 5′-CTGATGAATTCGTCGATTC GGTTGCAGCA-3′ and 5′-TATCAAGGGACCCTGTATCTGGGAA-3′ to amplify the reverse-transcribed TVCV RNA (350 bp) and primers 5′-CTGGCGACGCATCATTC-3′ and 5′-GAATTACCGCGGCTGCT-3′ to amplify 18S rRNA (301 bp).

RNA binding assays. The *MP^{TVCV}* and *MP$^{K210A/K212A}$* coding sequences were each cloned as translational fusions to the glutathione *S*-transferase (GST) coding sequence in pGEX-5X-1 (GE, Piscataway, NJ). GST-MP^{TVCV}, GST-MP$^{TVCV(K210A/K212A)}$, or GST was expressed in BL21 Rosetta cells by induction in 0.4 mM isopropyl-β-thiogalactopyranoside (IPTG) at 28°C, and cell lysates were prepared in lysis buffer (50 mM Tris-HCl, pH 8, 200 mM NaCl, 1 mM dithiothreitol [DTT], 1 mM phenylmethylsulfonyl fluoride [PMSF], 1 mg/ml lysozyme) as previously described (21). Insoluble GST-MP^{TVCV} and GST-MP$^{TVCV(K210A/K212A)}$ were obtained by centrifugation at 10,000 × *g* at 4°C for 10 min, following which pellets were washed twice by resuspension in 400 μl of wash buffer (50 mM Tris-HCl, pH 8, 200 mM NaCl, 10 mM EDTA, 0.5% Triton X-100, 1 mM DTT, 1 mM PMSF) and centrifugation at 10,000 × *g* at 4°C. Clarified lysates containing GST were used directly without purification on glutathione-Sepharose. To test for RNA binding, 1 μg of GST-MP^{TVCV} or GST-MP$^{TVCV(K210A/K212A)}$ pellets, or GST lysate, was resolved on 13.5% SDS-PAGE gels, and proteins were blotted to nitrocellulose and incubated with RNA as previously described (25). Fluorescein-labeled RNA was transcribed *in vitro* from the 1.85-kb *Xenopus laevis* EF1α gene, expressed from the SP6 promoter in pTRIPLEscript using the SP6 mMessage Machine kit (Life Technologies, Grand Island NY) and fluorescein RNA labeling mix (Roche, Mannheim, Germany) per the manufacturers' protocols. Following incubation of renatured protein blots with fluorescein-labeled RNA, RNA binding was visualized using the Typhoon system (GE, Piscataway, NJ) with 532-nm excitation and 526-nm short-pass emission filters.

Microscopy. Confocal laser scanning microscopy (CLSM) was performed using a Leica TCS SP5 spectral imaging system (Leica Microsystems, Wetzlar, Germany). GFP fluorescence was excited with a 488-nm argon laser, and emission was detected at 500 to 530 nm. RFP fluorescence was excited with a 561-nm diode-pumped solid-state (DPSS) laser, and emission was detected at 590 to 630 nm. Z series were collected at ~1-μm intervals and imaged using Leica software (Leica Microsystems). Three-dimensional (3D) imaging was done using Velocity software (Improvision, Coventry, United Kingdom). Virus infection sites on inoculated leaves were identified using an Olympus SZX-12 stereomicroscope (Olympus Corporation, Center Valley, PA). Green fluorescence was excited with a 480-/30-nm filter, and an emission 535-/40-nm filter was used for detection.

RESULTS

MP^{TVCV} localizes to PD and ER replication sites but not to microtubules. As a tool to investigate MP trafficking in *Arabidopsis* during virus infection, we constructed an infectious TVCV replicon, modeled after the approach used with TMV (6). To do this, we created a translational fusion of the *MP^{TVCV}* and *GFP* (or *RFP*) coding regions to express a C-terminal MP^{TVCV}-GFP fusion from the viral *MP* promoter. As in TMV, this fusion deleted the *CP* gene (Fig. 1A, TVCV::MP-GFP). Based on studies of the analogous TMV::MP-GFP (6), we expected TVCV::MP-GFP to be infectious and move cell to cell in inoculated leaves, thereby allowing us to examine the subcellular localization of MP^{TVCV}-GFP during the time course of virus infection in infection sites. However, without CP, TVCV::MP-GFP, like TMV::MP-GFP, would not systemically infect plants. To demonstrate the infectious nature of our TVCV::MP-GFP replicon clone and the function of the encoded MP^{TVCV}-GFP, we inoculated *N. benthamiana* leaves with TVCV::MP-GFP and used confocal microscopy to compare the resulting expanding fluorescent foci to those produced by the well-characterized TMV::MP-GFP (Fig. 1).

Similarly to TMV::MP-GFP (6, 26), TVCV::MP-GFP produced infection sites that appeared as fluorescent rings on inoculated leaves, in which GFP fluorescence was absent from the centers (late times in infection) (Fig. 1B). This suggested that MP^{TVCV}, like MP^{TMV}, accumulated during the course of infection but was degraded at late times in the TVCV life cycle. When we compared TVCV and TMV directly in *N. benthamiana*, confocal examination of MP^{TVCV}-GFP subcellular localization across these

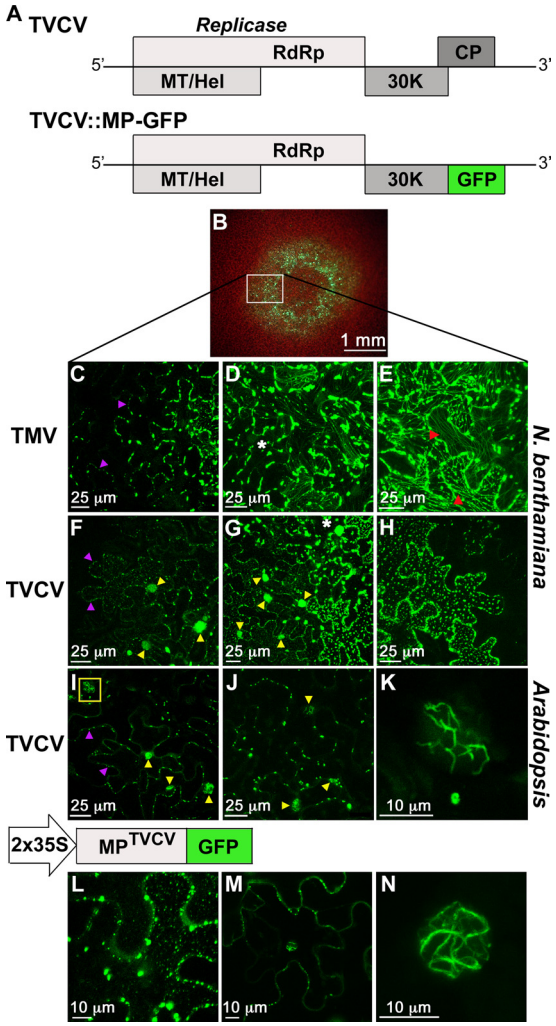

FIG 1 MP^{TVCV} localizes to the nucleus during virus infection. (A) Schematic representation of TVCV +RNA genome and the replicon TVCV::MP-GFP. (B) TVCV::MP-GFP expanding fluorescent foci on inoculated *N. benthamiana* leaf at 4 days p.i. are evident as a fluorescent ring and similar to infection sites produced by TMV::MP-GFP (6). The boxed area is the region magnified (left to right) in panels F to H. Equivalent regions of TMV::MP-GFP infection sites in *N. benthamiana* are shown in panels C to E. (C to J) CLSM-projected Z series of cells in fluorescent foci at 4 days p.i. on *N. benthamiana* leaves (C to H) or 7 days p.i. on *Arabidopsis* Col-0 leaves (I to K) inoculated with TMV::MP-GFP (C to E) or TVCV::MP-GFP (F to K). Cells at early (leading edge) (C, F, and I), middle (D, G, and J), and late (E and H) stages of infection are shown. (H) Black areas at right and bottom (E and H) are cells in which MP^{TVCV}-GFP was degraded and remained only at PD. Examples of MP^{TVCV}-GFP-containing nuclei (yellow arrowheads) and PD (purple arrowheads), MP^{TMV}-GFP colocalizing with microtubules (red arrowheads), and intracellular peripheral bodies (white asterisks) are marked. See the text for details. (K) Higher magnification of nucleus boxed in panel I showing MP^{TVCV}-GFP localizing to nuclear filaments. (L to N) Transient expression of MP^{TVCV}-GFP in agroinfiltrated *N. benthamiana* leaf cells at 40 h. CLSM-projected Z series show MP^{TVCV}-GFP localizing to PD and intracellular bodies at the cell periphery (L), PD and the nucleus at a midplane section (M), and a filamentous structure inside the nucleus (N).

infection sites showed that MP^{TVCV}-GFP recapitulated a number of the features of MP^{TMV}-GFP (Fig. 1C to H). Early in infection (first cells at the leading edge), MP^{TVCV}-GFP, like MP^{TMV}-GFP, localized to discrete punctae at the cell wall, which appear to be PD (27), and to motile intracellular vesicles, with the latter being more numerous in TVCV-infected cells (Fig. 1C and F). At this early time, both MP^{TVCV}-GFP and MP^{TMV}-GFP also localized to ER membrane-derived replication sites, which appeared to enlarge and accumulate MP at later stages of infection, based on their levels of fluorescence (Fig. 1C, D, F, and G). To show this, we inoculated a TVCV::MP-RFP replicon onto an *N. benthamiana* transgenic line that expressed the ER marker GFP-HDEL (22). As reported for MP^{TMV} (28), MP^{TVCV}-RFP colocalized with ER in small intracellular and larger peripheral bodies, which were formed at junctions of cortical ER tubules (Fig. 1D and G and 2A). As infection progressed, the ER network collapsed and these replication sites enlarged (Fig. 2B, D, G, H, and I). Consistent with these being replication sites, the peripheral bodies consisted of MP^{TVCV}-RFP engulfed by ER membrane (Fig. 2C). Upon complete collapse of the ER, these MP^{TVCV}-RFP replication sites remained associated with the fragmented ER (Fig. 2G, H, and I). Also like MP^{TMV}, MP^{TVCV} appeared to be degraded at the latest times in infection (focus centers) (Fig. 1H), at which point the ER network re-formed and MP^{TVCV} was found only at PD (punctae at the cell wall) (Fig. 1H and 2E and data not shown).

Despite these similarities to MP^{TMV}, we found that MP^{TVCV} differed from MP^{TMV} in three important respects. First, in contrast to the well-documented association of MP^{TMV} with microtubules (12, 29) (Fig. 1E), we found no association of MP^{TVCV} with microtubules when we inoculated TVCV::MP-RFP onto *N. benthamiana* transgenic plants that expressed a GFP fusion of *Arabidopsis* α-tubulin (TUA-GFP) (23), nor did we observe any rearrangement of microtubules (Fig. 1F to H and 2M and N). Second, when we inoculated TVCV::MP-RFP onto an *N. benthamiana* transgenic line expressing a talin-GFP fusion (19), we observed, at late stages of infection, distortion of the actin cytoskeleton and bundling of filamentous actin (F-actin) near and around MP^{TVCV}-marked replication sites that appeared to parallel changes in the ER membrane (Fig. 2F, J, K, and L). Third, in striking contrast to MP^{TMV}, MP^{TVCV}-GFP localized to nuclei in infected cells at the earliest stages and throughout infection up to the point of MP^{TVCV} degradation at the center of infection sites (Fig. 1F to H). To show that this unexpected nuclear accumulation of MP^{TVCV}-GFP was due to nuclear import of MP^{TVCV} and not diffusion of free GFP produced by truncation or protein degradation, we analyzed protein extracts from *N. benthamiana* leaves infected with our TVCV::MP-GFP and TMV::MP-GFP replicons on immunoblots using anti-GFP antibodies and did not detect any free GFP (data not shown). In addition, we found that MP^{TVCV} targets to nuclei in an NLS-dependent manner (see below).

The localization pattern of MP^{TVCV}-GFP in TVCV infection sites on *Arabidopsis* was the same as that on *N. benthamiana*, differing only in the temporal aspects of MP^{TVCV}-GFP distribution. In Col-0, MP^{TVCV}-GFP localized to intracellular and peripheral ER replication sites, in addition to PD and nuclei, at all stages in infection, from the earliest stages in cells at the infection front through the late stages up to the point of MP^{TVCV}-GFP degradation at the infection site center (Fig. 1I to K). As in *N. benthamiana*, MP^{TVCV}-GFP-associated peripheral ER sites expanded as infection progressed (Fig. 1I and J), MP^{TVCV}-GFP was found only at PD at the latest stage in infection (centers of foci) when MP^{TVCV}-GFP was degraded (Fig. 2O), and MP^{TVCV}-GFP did not distribute to microtubules (Fig. 1I and J).

Nuclear MP^{TVCV} localizes to novel F-actin-containing filaments that associate with chromatin. We observed that MP^{TVCV}-GFP localized to a novel filamentous nuclear compartment in

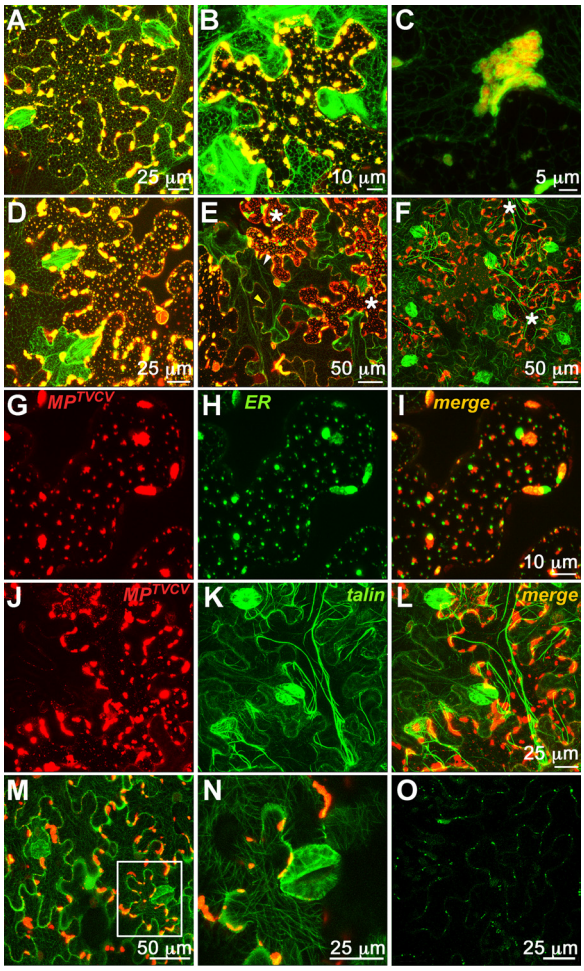

FIG 2 TVCV infection leads to collapse of the ER network and disruption of the actin cytoskeleton. (A to N) CLSM-projected Z series of cells from TVCV::MP-RFP-infected expanding fluorescent foci at 4 days p.i. on transgenic *N. benthamiana* lines expressing GFP-HDEL to label ER (A to E and G to I), talin-GFP to label the actin cytoskeleton (F, J, K, and L), or TUA-GFP to label microtubules (M and N). Cells at middle (A to C) or late (D to N) stages of infection are shown. Football-shaped ~25- by 30-μm areas densely labeled with GFP-HDEL (A and D), talin-GFP (F, K, and L), or TUA-GFP (M and N) are stomatal guard cells. (A) ER sites containing MP^{TVCV}-RFP at nodes in the reticular ER and at the cell periphery. (B and D) Progressive collapse of the reticulate ER and the subsequent enlargement of MP^{TVCV}-RFP ER sites in the cortical regions of the cell. (C) High-magnification image of MP^{TVCV}-RFP-containing ER site. (E) ER network re-forms (white arrowhead) at latest stages of infection when MP^{TVCV} is degraded and remains only at PD (yellow arrowhead). (F) Disruption of the actin cytoskeleton late in infection. Asterisks in panels E and F mark examples of cells that contain enlarged peripheral MP^{TVCV}-ER sites at late-stage infection before ER re-forms. (G to I) MP^{TVCV}-RFP and ER (GFP-HDEL) sites partition into visibly distinct compartments but remain associated with each other late in infection. (J to L) The actin cytoskeleton is disrupted late in TVCV infection, with actin filaments (talin-GFP) appearing to be distorted near, and bundle around, MP^{TVCV}-RFP-containing ER sites, but MP^{TVCV}-RFP does not distribute to microtubules, and the microtubule network is not perturbed (M and N). (N) Enlargement of boxed area in panel M. (O) CLSM-projected Z series of cells at center of TVCV::MP-GFP infection site on inoculated Col-0 leaves at 7 days p.i. As in TMV infection, MP^{TVCV}-GFP is downregulated at the center of infection sites and remains only at what appear to be PD (punctate spots along the cell periphery).

TVCV-infected cells in both *Arabidopsis* and *N. benthamiana* (Fig. 1F, G, I, and K and data not shown), in which, based on fluorescence intensity, it continued to accumulate as infection progressed, up to the latest stages in infection just prior to its being degraded (Fig. 1F to H). To show that this novel nuclear localization, as well as other differences from MP^{TMV} (Fig. 1F to H compared to C to E), was an intrinsic property of MP^{TVCV} *per se*, we transiently expressed MP^{TVCV}-GFP or MP^{TMV}-GFP, each driven by the 35S promoter, in *N. benthamiana* leaf cells using agroinfiltration (30). As we found for the early stages in TVCV infection, MP^{TVCV}-GFP, when expressed alone, localized to PD, numerous motile vesicles, intracellular and peripheral bodies, and the same nuclear filaments as those seen in TVCV-infected cells (Fig. 1L to N; see also Movie S1 in the supplemental material) and did not localize to microtubules. In contrast, MP^{TMV}-GFP, when expressed alone, localized to PD, intracellular bodies, and microtubules but did not localize to nuclei (data not shown), as previously reported (31). Importantly, we observed the same MP^{TVCV}-GFP-containing nuclear filaments in both Col-0 and *N. benthamiana* plants that were infected with our TVCV replicon or transiently expressed MP^{TVCV}-GFP (Fig. 1K and N). Thus, the localization of MP^{TVCV} to these novel nuclear filaments, as well as to PD, motile vesicles, and ER sites, was an intrinsic characteristic of this tobamovirus movement protein that did not require viral RNA or other viral components.

To more precisely localize these MP^{TVCV}-GFP-containing filaments within the nucleus, we used agroinfiltration to transiently express MP^{TVCV}-GFP in transgenic *N. benthamiana* lines that expressed RFP fusions of either histone 2B (H2B-RFP) to label chromatin or fibrillarin (FBL-RFP) to label nucleoli and Cajal bodies (19). MP^{TVCV}-GFP did not localize to nucleoli or to discrete FBL-RFP-labeled speckles (Cajal bodies) (Fig. 3A to C and data not shown). Rather, we found that MP^{TVCV}-GFP-containing filaments were associated with H2B-RFP-labeled chromatin, where MP^{TVCV}-GFP appeared to be in a filamentous network that contacted discrete regions of chromatin (Fig. 3D to L). These filaments bore a striking resemblance to polymerized nuclear actin that, in a recent study from the Gurdon lab, was shown to be required for transcriptional reactivation of the pluripotency gene *Oct4* when mouse cell nuclei are transplanted into the *Xenopus laevis* oocyte giant nucleus (germinal vesicle [GV]) (32). Thus, to determine whether MP^{TVCV}-GFP colocalized with F-actin in these nuclear filaments, we used agroinfiltration to transiently coexpress MP^{TVCV}-GFP and the calponin binding domain of utrophin (UtrCH) fused to TagRFP (TagRFP-UtrCH), a probe reported to faithfully mark F-actin without altering the balance of actin assembly/disassembly (18). TagRFP-UtrCH, when expressed alone, labeled the actin cytoskeleton and, when found in the nucleus, was diffuse throughout the nucleoplasm (Fig. 3Q). When it was coexpressed with MP^{TVCV}-GFP, TagRFP-UtrCH still labeled the actin cytoskeleton, but the nuclear TagRFP-UtrCH now colocalized with MP^{TVCV}-GFP in filaments (Fig. 3M to O). Thus, these chromatin-associated nuclear filaments contain both MP^{TVCV} and F-actin.

MP^{TVCV} contains an NLS that is required for import into the nucleus. Our inspection of the MP^{TVCV} sequence identified a potential classic basic monopartite nuclear localization sequence at amino acid (aa) residues 209 to 214 (RKRKKK) (Fig. 3P and 4). Aligning the MP sequences from different tobamoviruses, we found that this putative NLS appeared to be conserved in all sub-

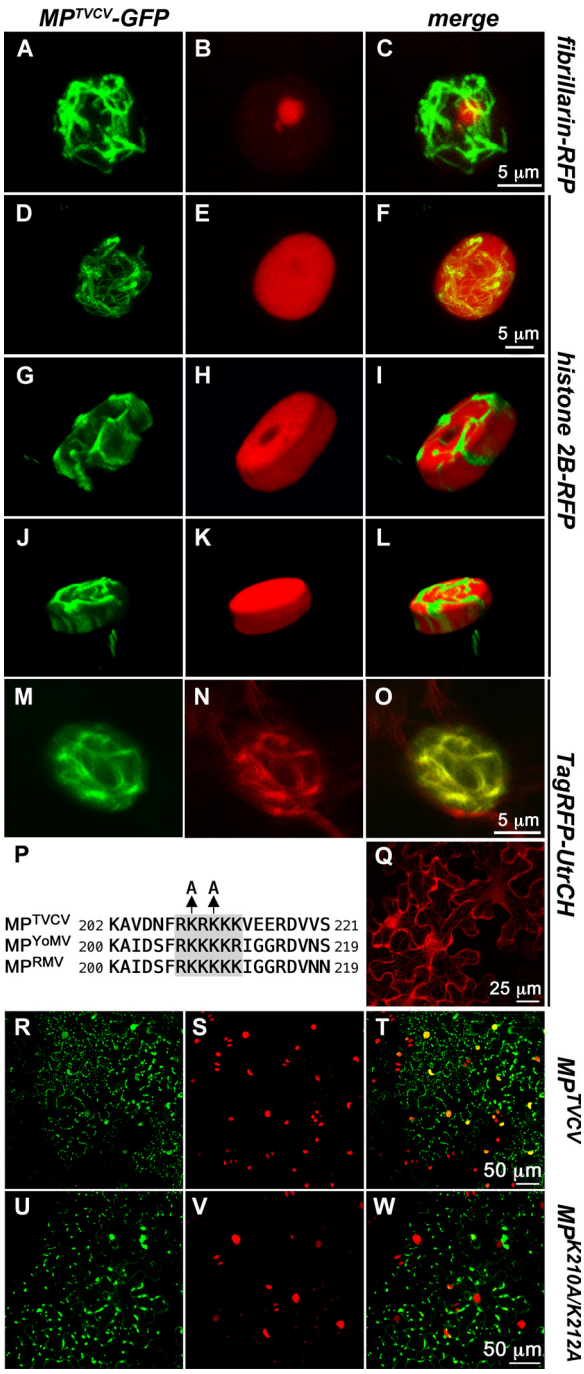

FIG 3 MP^{TVCV}-GFP localizes in an NLS-dependent manner to actin-containing nuclear filaments that appear to contact discrete regions of chromatin. (A to O) CLSM-projected Z series of nuclei from agroinfiltrated *N. benthamiana* leaf cells transiently expressing MP^{TVCV}-GFP. Shown are transgenic *N. benthamiana* plants expressing fibrillarin-RFP (nucleolus and Cajal bodies) (A to C) or histone 2B (H2B)-RFP (chromatin) (D to L) or wt plants agroinfiltrated to coexpress TagRFP-UtrCH (M to O). MP^{TVCV}-GFP (green), fibrillarin-RFP, H2B-RFP, TagRFP-UtrCH (red), and the corresponding superimposed images are shown. (G to L) Projected Z-plane 5-μm sections from the middle (G to I) and bottom (J to L) of the nucleus shown in panels D to F. (M to O) MP^{TVCV}-GFP and TagRFP-UTR colocalize to the nuclear filaments in MP^{TVCV}-expressing cells. (Q) TagRFP-UtrCH transiently expressed alone in *N. benthamiana* leaf cells labels the actin cytoskeleton and, when found in nuclei, is diffuse in the nucleoplasm. (P) Alignment of MP^{TVCV}, MP^{YoMV}, and MP^{RMV} protein sequences showing conservation of basic residues (gray shading) of the monopartite NLS at the position corresponding to residues 209 to 214 of MP^{TVCV}. Locations of the two Lys-to-Ala mutations in MP$^{TVCV(K210A/K212A)}$ are shown. (R to W) CLSM-projected Z series of leaves from transgenic *N. benthamiana* plants expressing histone 2B-RFP and inoculated with the replicon TVCV::MP-GFP (R to T) or TVCV::MP$^{K210A/K212A}$-GFP (U to W). Shown are MP^{TVCV}-GFP (green) (R), MP$^{TVCV(210A/212A)}$-GFP (green) (U), and histone 2B-RFP (red) (S and V) and the corresponding superimposed images (T and W). MP^{TVCV}-GFP localizes to nuclei (yellow-orange in panel T), but MP$^{TVCV(210A/212A)}$-GFP does not (nuclei are red only in panel W).

group 3 tobamoviruses but was not present in the viruses in subgroup 1 or 2, including TMV, save for *Tobacco mild green mosaic virus* (TMGMV) and *Sunn-hemp mosaic virus* (SHMV), both in subgroup 1 (Fig. 4; see also Fig. S1 in the supplemental material; other data not shown).

To determine if MP^{TVCV} amino acid residues 209 to 214 were, in fact, an NLS, we mutated the Lys residues at positions 210 and 212 to Ala and introduced this mutation into our infectious replicon to create TVCV::MP$^{K210A/K212A}$-GFP (Fig. 3P). We then inoculated the transgenic *N. benthamiana* line that expressed H2B-RFP with this or with our wt TVCV::MP-GFP replicon. We found that TVCV::MP$^{K210A/K212A}$-GFP was still infectious, producing expanding fluorescent foci on inoculated leaves (Fig. 5C). In wt TVCV::MP-GFP-infected sites, MP^{TVCV}-GFP clearly localized with H2B-RFP in nuclei throughout the infection sites, in addition to its cytoplasmic distribution among PD, motile vesicles, and ER replication sites (Fig. 3R to T). In contrast, MP$^{TVCV(K210A/K212A)}$-GFP did not enter the nucleus, as evident from our finding that it did not localize to H2B-RFP-marked nuclei (Fig. 3U to W). Thus, MP^{TVCV} residues 209 to 214 act as a functional NLS that is essential for MP^{TVCV} import into the nucleus. Our MP^{TVCV} NLS mutant still localized to PD, vesicles, and ER replication sites in TVCV::MP$^{K210A/K212A}$-GFP-infected sites. The only difference that we observed from wt MP^{TVCV}-GFP was that the number of intracellular bodies and ER sites, and the accumulation of MP$^{TVCV(K210A/K212A)}$-GFP at these sites, as assessed by fluorescence intensities, appeared to be increased (Fig. 3R and U).

Nuclear MP^{TVCV} is necessary for efficient TVCV infection. TVCV::MP$^{K210A/K212A}$-GFP infection sites displayed the same progression of infection as we observed in wt TVCV sites, with MP$^{TVCV(K210A/K212A)}$-GFP being degraded at the latest stage of infection. However, when we inoculated *N. benthamiana* plants with our MP^{TVCV} NLS mutant TVCV::MP$^{K210A/K212A}$-GFP, it was evident that the expanding foci were smaller than those produced by wt TVCV::MP-GFP (Fig. 5B and C). To quantify this, we measured the sizes of expanding TVCV::MP-GFP and TVCV::MP$^{K210A/K212A}$-GFP foci on inoculated leaves at 5 days p.i. Wild-type TVCV::MP-GFP infection sites were about twice the area of TVCV::MP$^{K210A/K212A}$-GFP infection sites (4.5 ± 0.2 mm^2 versus 2.2 ± 0.1 mm^2, $P < 0.0001$) (Fig. 5A). This suggested that a functional MP^{TVCV} NLS was necessary for efficient TVCV cell-to-cell spread.

To examine this further, we analyzed the consequences of mutating the MP^{TVCV} NLS for TVCV systemic infection in *N. benthamiana* and *Arabidopsis*. To do this, we introduced the NLS mutation into the fully infectious wt TVCV genome that expressed untagged MP to produce TVCV$^{MP(K210A/K212A)}$. As shown in Fig. 5, TVCV$^{MP(K210A/K212A)}$ systemic spread was inhibited in *N. benthamiana*, based on both the percentage of infected plants and

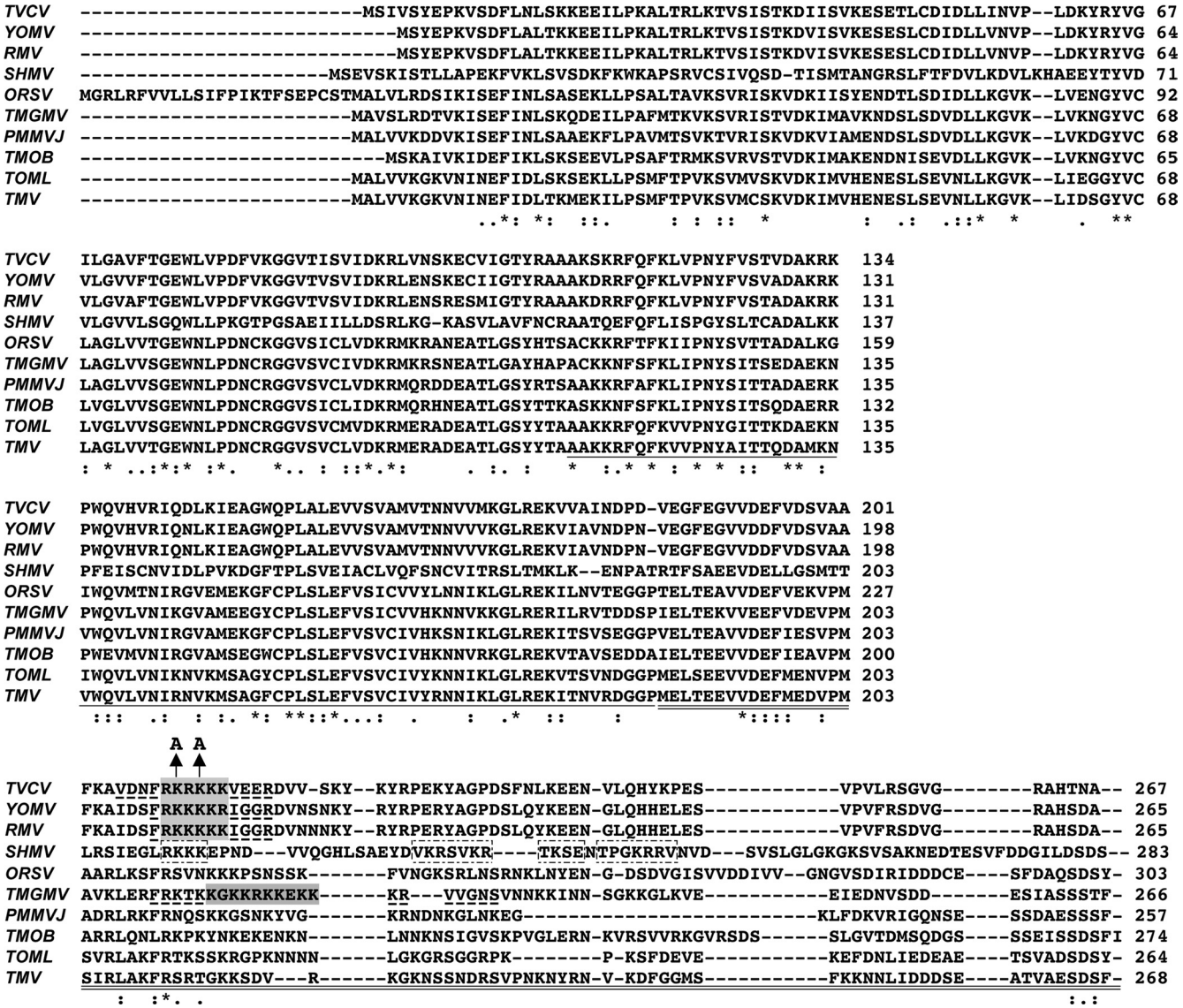

FIG 4 The MP^{TVCV} NLS appears to be conserved among subgroup 3 tobamoviruses. Alignment of MP protein sequences from the subgroup 3 tobamoviruses (TVCV, YoMV, and RMV) and representative subgroup 1 tobamoviruses, including TMV (shown at bottom). The basic residues in the MP^{TVCV} monopartite NLS are shaded in gray, with the two missense mutations in MP$^{TVCV(K210A/K212A)}$ indicated. The corresponding predicted monopartite NLSs in YoMV and RMV are also shown with basic residues shaded in gray, as is a predicted monopartite NLS in TMGMV. Broken lines indicate additional residues predicted to be part of the NLS interaction domain with importin-α (cNLS Mapper, http://nls-mapper.iab.keio.ac.jp/cgi-bin/NLS_Mapper_form.cgi//). Boxed in SHMV are residues predicted to comprise a potential extended bipartite NLS. Single and double lines beneath the MP^{TMV} sequence mark the two extended RNA binding regions identified in TMV (33). Sequence similarity is indicated below the aligned sequences. TVCV, *Turnip vein clearing virus* (accession no. Q88921); YoMV, *Youcai mosaic virus* (same as ORMV, *Oilseed rape mosaic virus*; accession no. Q66221); RMV, *Holmes ribgrass mosaic virus* (accession no. Q9QDI8); SHMV, *Sunn-hemp mosaic virus* (accession no. P03585); ORSV, *Odontoglossum ringspot virus*, strain Japan (accession no. P22590); TMGMV, *Tobacco mild green mosaic virus* (TMV U2 strain; accession no. P18338); PMMVJ, *Pepper mild mottle virus*, strain Japan (accession no. P89658); TMOB, *Tobamovirus Ob* (also known as *Obuda pepper virus*; accession no. Q83485); ToML, *Tomato mosaic virus*, strain L (also known as TMV strain tomato; accession no. P69513); TMV, *Tobacco mosaic virus*, strain U1 (accession no. P03583). Numbers to the right of each sequence indicate residue position within the protein.

the systemic accumulation of TVCV CP at different days p.i. TVCV$^{MP(K210A/K212A)}$-infected plants exhibited a significant delay ($P < 0.0001$) in the onset of systemic disease symptoms, compared to plants infected with wt TVCV (Fig. 5E; Table 1), and displayed attenuated disease symptoms (Fig. 6). Fitting with this, the systemic accumulation of CP was also delayed. Viral CP was clearly detected at 4 days and 8 days p.i. in systemic leaf extracts from ~75% and 100%, respectively, of wt TVCV-infected *N. benthamiana* plants. In contrast, CP was rarely detected, and then at only very low levels, in TVCV$^{MP(K210A/K212A)}$-infected *N. benthamiana* systemic leaves at 4 days p.i., and by 8 days p.i., although present in all plants tested, CP had accumulated to lower levels than those in wt TVCV-infected plants (Fig. 5D). We obtained the same results in *Arabidopsis*. As TVCV produces mild disease symptoms in Col-0 plants, we assessed systemic infection in this host by assaying the accumulation of TVCV CP in extracts of systemic leaves. TVCV$^{MP(K210A/K212A)}$ systemic spread, compared to that of wt TVCV, was significantly delayed in Col-0 plants,

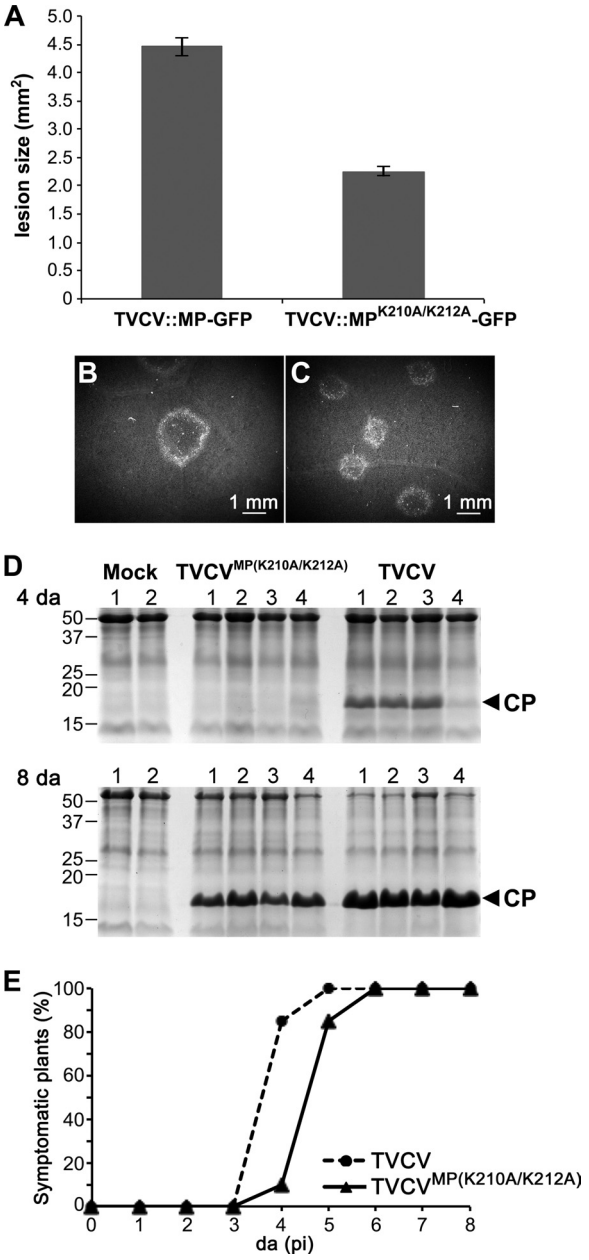

FIG 5 The NLS mutant TVCV$^{MP(K210A/K212A)}$ is delayed in local spread and systemic infection in *N. benthamiana*. (A) Areas of infection sites at 5 days p.i. on *N. benthamiana* leaves inoculated with replicon TVCV::MP-GFP or TVCV::MP$^{K210A/K212A}$-GFP. The areas of 102 TVCV::MP-GFP and 131 TVCV::MP$^{K210A/K212A}$-GFP infection sites on leaves inoculated with a standardized amount of RNA (see Materials and Methods) were measured. (B and C) Representative infection sites produced by TVCV::MP-GFP (B) or TVCV::MP$^{K210A/K212A}$-GFP (C) on *N. benthamiana* leaves at 5 days p.i. (D) Coomassie blue-stained SDS-PAGE gels of systemic leaf extracts from *N. benthamiana* plants inoculated with full-length infectious TVCV$^{MP(K210A/K212A)}$ (NLS mutant) or with wt TVCV or mock inoculated at 4 days and 8 days p.i. Equal amounts of extract from 1-cm punches of systemic leaves were analyzed in each gel (see Materials and Methods). Positions of CP (17 kDa) and of protein markers (kDa) are marked. (E) Time course of appearance of systemic disease symptoms on *N. benthamiana* plants inoculated with equal amounts of wt TVCV or the NLS mutant TVCV$^{MP(K210A/K212A)}$ (Table 1, trial 1).

TABLE 1 TVCV infectivity on *N. benthamiana*[a]

Trial	Inoculum	% of total inoculated plants at day postinoculation: 1	2	3	4	5	6	7	8
1	wt	0	0	0	85	100	100	100	100
	TVCV$^{MP(K210/K212A)}$	0	0	0	10	85	100	100	100
	Mock	0	0	0	0	0	0	0	0
2	wt	0	0	10	85	100	100	100	100
	TVCV$^{MP(K210/K212A)}$	0	0	0	10	80	100	100	100
	Mock	0	0	0	0	0	0	0	0
3	wt	0	0	0	90	100	100	100	100
	TVCV$^{MP(K210/K212A)}$	0	0	0	15	90	100	100	100
	Mock	0	0	0	0	0	0	0	0

[a] Symptomatic plants as percentage of total inoculated plants (20 per assay). Nonparametric survival analysis with right censoring (Wilcoxon test statistic), $P < 0.0001$ for 3 trials shown.

based on the systemic accumulation of TVCV CP at different days p.i. (Fig. 7; Table 2; $P < 0.001$), and this NLS mutant also produced attenuated disease symptoms, compared to wt TVCV, in Col-0 plants (Fig. 6).

To show that this delay in local and systemic virus spread was specifically due to the absence of a nuclear function of MP^{TVCV}, and not the result of an effect of the NLS mutation in MP$^{TVCV(K210A/K212A)}$ on virus replication or cell-to-cell movement *per se*, we examined the ability of MP$^{TVCV(K210A/K212A)}$ to bind RNA and traffic cell to cell, the latter as a means to assess its effects on PD gating, and assayed the replication of

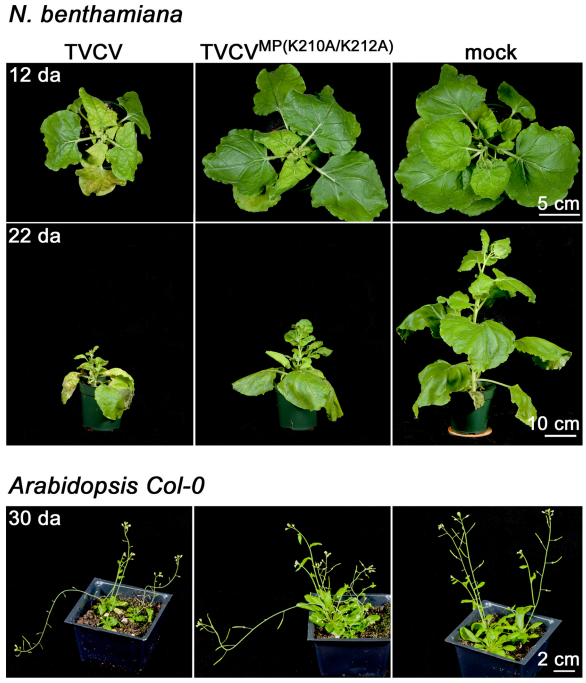

FIG 6 The NLS mutant TVCV$^{MP(K210A/K212A)}$ produces attenuated disease symptoms in *N. benthamiana* and *Arabidopsis* Col-0. *N. benthamiana* (top) or Col-0 (bottom) plants at 12 days or 22 days (*N. benthamiana*) or 30 days (Col-0) postinoculation with wt TVCV or TVCV$^{MP(K210A/K212A)}$, or mock inoculated, as indicated.

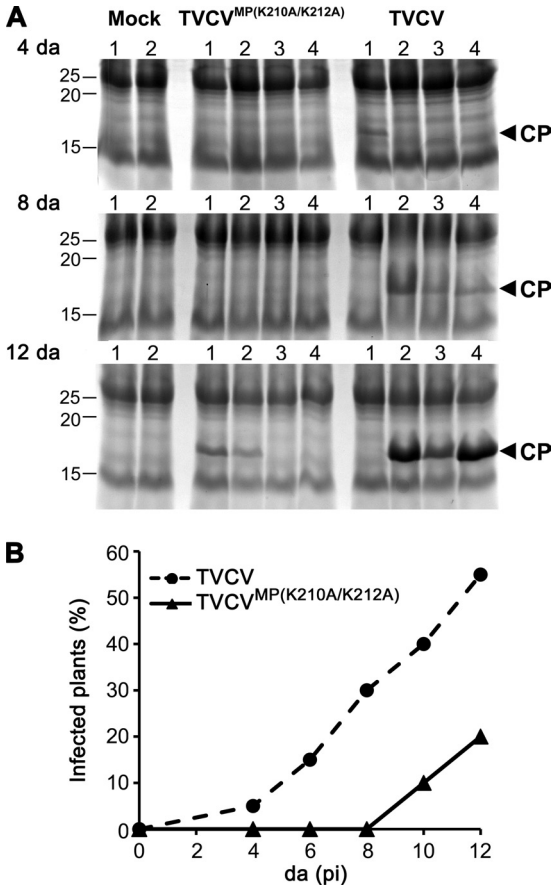

FIG 7 The NLS mutant TVCV$^{MP(K210A/K212A)}$ is delayed in systemic infection in *Arabidopsis* Col-0. (A) Coomassie blue-stained SDS-PAGE gels of systemic leaf extracts from Col-0 plants inoculated with full-length infectious TVCV$^{MP(K210A/K212A)}$ (NLS mutant) or with wt TVCV or mock inoculated at 4 days, 8 days, and 12 days p.i. Equal amounts of systemic leaf tissue extracts (0.5 g/ml) were analyzed in each gel (see Materials and Methods). Positions of CP (17 kDa) and of protein markers (kDa) are marked. (B) Development of systemic disease as assessed by CP accumulation in Col-0 plants inoculated with equal amounts of wt TVCV or the NLS mutant TVCV$^{MP(K210A/K212A)}$ (Table 2, trial 1).

TVCV$^{MP(K210A/K212A)}$ in *N. benthamiana* protoplasts. The C-terminal half of MP^{TMV} contains two extended RNA binding domains (33). Based on our sequence alignments, the MP^{TVCV} NLS (residues 209 to 214) is within the second of these domains (Fig. 4). To exclude the possibility that our NLS mutant MP$^{TVCV(K210A/K212A)}$ was defective in RNA binding, we used a membrane binding assay to test GST fusions of both MP$^{TVCV(K210A/K212A)}$ and wt MP^{TVCV} for their ability to bind single-stranded RNA (ssRNA) *in vitro*. As shown in Fig. 8, MP$^{TVCV(K210A/K212A)}$ bound ssRNA *in vitro* to the same extent as did wt MP^{TVCV}. This binding was specific for MP^{TVCV}, as free GST did not bind ssRNA when tested in this same assay (Fig. 8A).

To directly examine the ability of the NLS mutant to traffic between cells, we used agroinfiltration to transiently express MP$^{TVCV(K210A/K212A)}$-GFP and wt MP^{TVCV}-GFP in *N. benthamiana* leaf epidermal cells, using an established assay (21). We infiltrated a low concentration of each *A. tumefaciens* culture so that each movement protein would be expressed in individual isolated cells (~1 in 10) by ~24 h p.i. (21), and then we assessed MP cell-to-cell trafficking over time by using CLSM to count the numbers of cells in individual foci at 44 to 46 h p.i. As shown in Table 3, the NLS mutant MP$^{TVCV(K210A/K212A)}$ -GFP trafficked cell to cell at least as well as did wt MP^{TVCV}-GFP, if not slightly more efficiently (Table 3). Thus, this NLS mutation did not impair the two key activities of MP$^{TVCV(K210A/K212A)}$ that are essential for its function in virus movement, namely, its ability to bind ssRNA (Fig. 8A) and to traffic cell to cell (Table 3).

To exclude the possibility that the NLS mutation in MP$^{TVCV(K210A/K212A)}$ affected virus replication, we transfected *N. benthamiana* protoplasts with full-length genomic (+RNA) transcripts of wt TVCV or the NLS mutant TVCV$^{MP(K210A/K212A)}$ and assayed virus replication by sqRT-PCR, using reverse transcription primers specific for the TVCV −RNA strand to ensure that we quantified virus replication and not the subsequent transcription of viral mRNA. We detected no viral RNA by sqRT-PCR immediately following transfection, which established both the baseline for our assay and the specificity of our reverse transcription primer for TVCV −RNA (Fig. 8B, 0 h). At 4 h and 20 h posttransfection, we detected increasing amounts of viral RNA, with the NLS mutant TVCV$^{MP(K210A/K212A)}$ and wt TVCV replicating to the same levels (Fig. 8B). Thus, the NLS mutant MP$^{TVCV(K210A/K212A)}$ does not have a direct effect on TVCV replication, and MP$^{TVCV(K210A/K212A)}$ properly localizes to ER sites and PD, traffics cell to cell, and binds RNA (Fig. 3U to W and 8; Table 3). Furthermore, the phenotype of MP$^{TVCV(K210A/K212A)}$ in delaying TVCV spread is independent of virus encapsidation since this delay is exhibited by both the replicon TVCV::MP$^{K210A/K212A}$, which does not encode CP, and by the mutated full-length virus TVCV$^{MP(K210A/K212A)}$ (Fig. 5 to 7). Based on our results, we conclude that MP^{TVCV} targets to the nucleus, where it localizes to F-actin-containing filaments that associate with chromatin to provide a function that is necessary for efficient TVCV spread and systemic infection.

DISCUSSION

MP^{TMV} is one of the most extensively characterized plant virus movement proteins and has been the model for understanding how a single movement protein can execute multiple functions to regulate virus genome transport within and between cells (7, 34).

TABLE 2 TVCV infectivity on *Arabidopsis* Col-0[a]

Trial	Inoculum	% total inoculated plants at day postinoculation: 1	2	3	4	6	8	10	12
1	wt	0	0	0	5	15	30	40	55
	TVCV$^{MP(K210/K212A)}$	0	0	0	0	0	0	10	20
	Mock	0	0	0	0	0	0	0	0
2	wt	0	0	0	6.25	25	50	75	ND[b]
	TVCV$^{MP(K210/K212A)}$	0	0	0	0	0	12.5	25	ND
	Mock	0	0	0	0	0	0	0	ND
3	wt	0	0	0	0	15	35	55	75
	TVCV$^{MP(K210/K212A)}$	0	0	0	0	0	5	25	35
	Mock	0	0	0	0	0	0	0	0

[a] Infected plants as percentage of total inoculated plants (20 per assay), based on presence of TVCV CP in extracts of systemic leaves (see Materials and Methods). Nonparametric survival analysis with right censoring (Wilcoxon test statistic), $P < 0.001$ for 3 trials shown.
[b] ND, not determined.

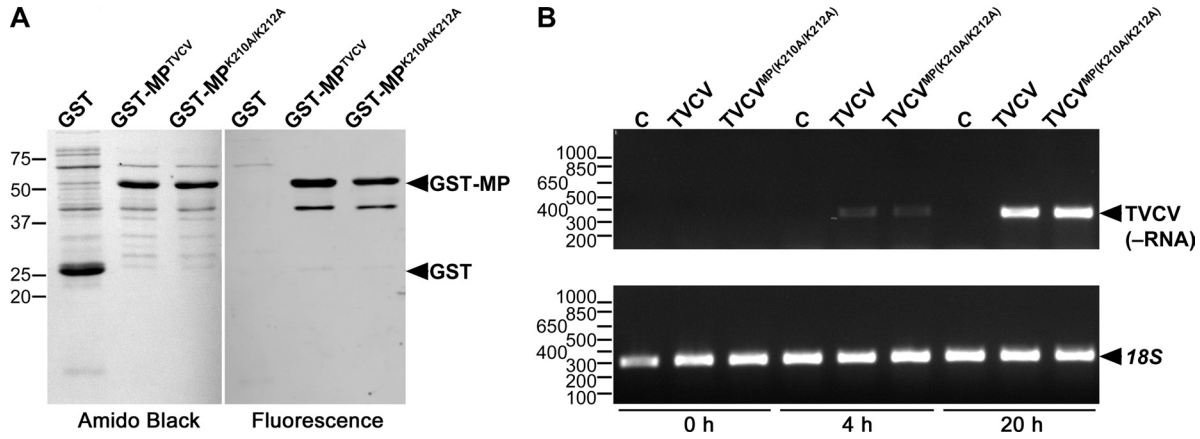

FIG 8 The NLS mutant MP$^{TVCV(K210A/K212A)}$ is not defective in ssRNA binding *in vitro* or in virus replication. (A) SDS-PAGE renatured gel blots of *E. coli*-expressed GST-MP^{TVCV}, GST-MP$^{TVCV(K210A/K212A)}$ or GST, as labeled, incubated with fluorescein-labeled EF1α RNA *in vitro* and then stained with amido black to detect proteins. Positions of GST-MP (56 kDa) and GST (26 kDa) and of protein markers (kDa) are marked. (B) Replication of wt TVCV and TVCV$^{MP(K210A/K212A)}$ (NLS mutant) in *N. benthamiana* protoplasts. Virus replication at 0, 4, and 20 h posttransfection, as indicated, was detected by RT-PCR using primers specific for the TVCV −RNA strand (see Materials and Methods). Positions of amplified TVCV −RNA fragment and 18S RNA loading control, and of DNA markers (nt), are marked. C, mock-transfected control.

However, *Arabidopsis thaliana* is, in general, a poor host for TMV. In contrast, TVCV efficiently infects *Arabidopsis*, including the Col-0 ecotype, and hence is the tobamovirus of choice for studies in this model plant to take advantage of its genetic, genomic, and molecular and cell biological resources. A key problem, which contributes to current confusion in the field, is the unproven assumption that the TVCV and TMV life cycles, including the localization of MP^{TVCV} and MP^{TMV} to virus replication sites and subcellular compartments, are the same. We have used an infectious clone of TVCV that encodes a functional MP^{TVCV}-GFP fusion to directly compare the distributions of MP^{TVCV} and MP^{TMV} during virus infection. Our results, reported here, showed that MP association with PD and with ER sites and its degradation at late stages were common features of infection by both TVCV and TMV, thereby underscoring the importance of these associations, and the regulation of MP levels, for tobamovirus replication and intercellular trafficking (Fig. 1 and 2). Importantly, we identified three striking features that distinguished TVCV infection from that of TMV.

Unlike MP^{TMV}, which redistributes from viral ER-associated replication sites to microtubules at late stages in infection, MP^{TVCV} accumulated in an unknown compartment that remained adjacent to these ER sites, and it did not redistribute to microtubules (Fig. 1 and 2E, G, H, and I). A second difference from TMV was that these late changes in ER were accompanied by a marked rearrangement and bundling of the actin cytoskeleton near and around these ER/MP^{TVCV} sites (Fig. 2F, J, K, and L). Thus, while the role of microtubules in promoting TMV cell-to-cell movement, or targeting MP^{TMV} for degradation, late in infection is still debated (29, 35), our studies did not identify a role for MP^{TVCV}-microtubule associations in TVCV infection, at least in terms of a redistribution of MP^{TVCV} to microtubules or obvious tracking of MP^{TVCV} along microtubules. In contrast, our findings did demonstrate distortion of the actin cytoskeleton late in infection at times when apparent TVCV replication sites enlarged to form compartments that remained adjacent to sites of collapsed ER membrane (Fig. 1 and 2). This, again, is distinct from TMV, where disruption of the microfilament network has not been observed (29). These differences between TVCV and TMV are consistent with other studies that indicate differing requirements for microtubules and microfilaments in infection by these two tobamoviruses. MP^{TMV} has been reported to bind to F-actin and to tubulin *in vitro* (36). Although the actin cytoskeleton is not obviously rearranged or morphologically altered during TMV infection, and the significance of MP^{TMV} interactions with microfilaments remains uncharacterized, imaging studies, combined with gene silencing and the use of inhibitory drugs such as latrunculin B, do point to a role for the actin cytoskeleton and myosin

TABLE 3 Cell-to-cell trafficking of MP^{TVCV} and MP$^{TVCV(K210A/K212A)}$

Trial	Protein[a]	Total foci[b] (total no. of fluorescent cells)	No. of foci[c] (% total foci)				P^d
			1 cell	2–7 cells	8–13 cells	≥14 cells	
1	MP^{TVCV}	30 (249)	1 (3.3)	12 (40.0)	15 (50.0)	2 (6.7)	
	MP$^{TVCV(K210A/K212A)}$	29 (329)	1 (3.4)	4 (13.8)	17 (58.6)	7 (24.1)	<0.05
2	MP^{TVCV}	31 (252)	1 (3.2)	14 (45.2)	12 (38.7)	4 (12.9)	
	MP$^{TVCV(K210A/K212A)}$	32 (340)	0 (0.0)	8 (25.0)	18 (56.3)	6 (18.8)	<0.05

[a] Vectors encoding GFP fusions of MP^{TVCV} or MP$^{TVCV(K210A/K212A)}$ were agroinfiltrated into *N. benthamiana* leaves. Shown are 2 separate trials.
[b] Total number of fluorescent foci counted.
[c] The number of foci in which each movement protein was in a single cell (1 cell) or had moved to 2 to 7, 8 to 13, or ≥14 cells.
[d] *P*, *t* test statistic.

motors in promoting TMV intercellular movement, in terms of both the TMV genome complexed with the viral 126-kDa replicase and host factors trafficking along microfilaments, and MP^{TMV} reaching PD (12, 37–39). In particular, TMV cell-to-cell spread, as assessed by the sizes of infection sites produced on *N. benthamiana* leaves, is inhibited by latrunculin B, which inhibits actin polymerization, or by silencing host actin or myosin XI-2 (37–39). In this same assay, latrunculin B also inhibits the intercellular spread of the potexvirus *Potato virus X* and the tombusvirus *Tomato bushy stunt virus*. However, neither latrunculin B nor silencing of myosin XI-2 or three other myosin isoforms was found to inhibit the cell-to-cell spread of TVCV. Similarly, the microtubule inhibitor oryzalin does not inhibit TVCV cell-to-cell spread (37). The cytoskeletal rearrangements that we observed during TVCV infection are intriguing in light of our finding that MP^{TVCV} localizes to nuclear F-actin filaments (Fig. 3). They may be related to MP^{TVCV} inducing or stabilizing nuclear F-actin filaments and consequently perturbing the balance of cytoplasmic G- and F-actin and would be consistent with the lack of an effect of latrunculin B on TVCV cell-to-cell spread (37). Fitting with this suggestion, we found that expressing very high levels of the TagRFP-UtrCH probe, which strongly binds to actin, interfered with the formation of nuclear MP^{TVCV}-containing F-actin filaments (data not shown). Whatever the explanation, our findings further underscore important differences in the involvement of microtubules and microfilaments in TMV and TVCV infection.

The most conspicuous and surprising difference from MP^{TMV} was that MP^{TVCV} targeted, in an NLS-dependent manner, to the nuclei of infected cells at all stages of infection, where it accumulated in novel F-actin-containing filaments that were associated with chromatin (Fig. 1 and 3). Our mutational analyses identified a classic basic monopartite NLS in MP^{TVCV} at amino acid residues 209 to 214, which was necessary and sufficient for targeting MP^{TVCV} to nuclei (Fig. 3 and 4), and also necessary for efficient TVCV local spread and systemic infection in both *Arabidopsis* Col-0 and *N. benthamiana* plants (Fig. 5 to 7). This NLS appears to be conserved among the subgroup 3 tobamoviruses comprising TVCV, YoMV/ORMV, and RMV, all of which infect plants in the Brassicaceae family, such as *Arabidopsis* and turnips. In addition, our comparison of the MP sequences for all reported subgroup 3 virus isolates showed that any amino acid substitutions within this sequence are Arg/Lys and Lys/Arg swaps that would preserve its character as a basic monopartite NLS (Fig. 4; see also Fig. S1 in the supplemental material).

Tobamoviruses appear to be ancient virus lineages. Based on phylogenetic analyses, it has been suggested that subgroup 1 and 2 tobamoviruses may have codiverged with their hosts (solanaceous plants for subgroup 1 and cucurbits and legumes for subgroup 2), but the subgroup 3 viruses likely arose from a subgroup 1 virus jumping into *Brassica* species (14). In contrast to the apparently conserved NLS, which we identified among the subgroup 3 tobamoviruses, our *in silico* analyses and use of three different algorithms (cNLS Mapper, WoLF PSort, and NucPred) did not predict any NLSs in the MPs encoded by the subgroup 1 or 2 viruses, including the well-characterized U1 strain of TMV (Fig. 4 and data not shown), save for SHMV (amino acid residues 211 to 214, 230 to 240, and 242 to 248) and one isolate of TMGMV (also known as TMV U2 strain, P18338, amino acid residues 214/215 to 224) (40, 41) (Fig. 4; see also Fig. S2 in the supplemental material). Intriguingly, the SHMV basic residues at positions 211 to 214, which may be part of a putative bipartite NLS, and the predicted TMGMV NLS are also conserved in terms of their position within the viral MP (Fig. 4). SHMV appears to be a recombinant between subgroup 1 and 3 viruses (14), which could explain the presence of the predicted NLS. The situation is more complex for TMGMV in that the MP encoded by three other isolates, referred to as strains U2 (EMBL/GenBank/DDBJ accession no. A4LAL8), Japanese (42), and HP (accession no. A3QVG8), is nearly identical in sequence to that reported by Nejidat et al. (98.8% similar and 96.1% identical) (40), except for what appears to be a deletion of the predicted NLS (see Fig. S2). Thus, although this sequence does not appear to be essential for TMGMV infection and viability, it does raise the question of whether a virus similar to the TMGMV strain that encodes the MP with a putative NLS (40, 41) was the progenitor of the subgroup 3 tobamoviruses.

Our extensive characterization of the NLS mutant $MP^{TVCV(K210A/K212A)}$ identified a single clear defect in this mutated MP: $MP^{TVCV(K210A/K212A)}$ was defective in nuclear targeting (Fig. 3). Compared to wild-type MP^{TVCV}, $MP^{TVCV(K210A/K212A)}$ was not altered in its localization to PD, motile vesicles, and ER replication sites (Fig. 3). $MP^{TVCV(K210A/K212A)}$ also was not defective in its two essential functions for virus movement, namely, binding ssRNA and its ability to alter PD, as assessed by its trafficking between cells (Fig. 8A; Table 3), nor did this NLS mutation directly affect virus replication (Fig. 8B). In addition, the effect of $MP^{TVCV(K210A/K212A)}$ on virus infection was independent of encapsidation since both the mutant replicon TVCV::$MP^{K210A/K212A}$-GFP, which does not encode CP, and the full-length mutant virus $TVCV^{MP(K210A/K212A)}$ encoding CP exhibited a significant delay in virus spread (Fig. 5 to 7; Tables 1 and 2). Thus, having eliminated direct effects on ER and PD targeting, (viral) RNA binding, cell-to-cell transport, replication, and encapsidation, our results strongly argue that MP^{TVCV} provides an important function in the nucleus, one which is necessary to promote virus spread and systemic infection, and appears to have evolved in the subgroup 3 tobamoviruses. Furthermore, this nuclear function of MP^{TVCV} does not require viral RNA or other TVCV components since MP^{TVCV}-GFP targeted to the same novel nuclear filaments in TVCV-infected *Arabidopsis* Col-0 and *N. benthamiana* leaf cells or when it was transiently expressed alone (Fig. 1 and 3).

What could be this nuclear function of MP^{TVCV}? Independent of their essential roles in genome trafficking, movement proteins can also redirect cellular activities to favor virus multiplication, including acting as virulence factors to block host defenses and thereby determining pathogenicity on different hosts (43, 44). One movement protein (TGB1) of *Potato virus X* acts to suppress gene silencing to block the host small interfering RNA (siRNA) defense (3, 45). The tobamovirus *Tomato mosaic virus* (ToMV) MP^{ToMV} can act as an effector to block pathogen-associated molecular pattern (PAMP)-triggered immunity or to induce effector-triggered immunity in plants with the Tm-2 resistance gene (46). The latter may involve MP^{ToMV} interacting with the transcription factors KELP and MBF1 (47, 48). The nuclear shuttle movement protein NSP encoded by the geminivirus *Cabbage leaf curl virus*, which transports viral genomes between the nucleus and cytoplasm, can interact with plasma membrane receptor-like kinases to suppress host defense (49, 50). It also redirects a host nuclear acetyltransferase to regulate genome encapsidation versus nuclear export, which may reprogram cells to support virus replication as well (51, 52). Our results suggest that nuclear MP^{TVCV} behaves like a virulence factor. It was necessary, but not sufficient, for virus

infection: TVCV that expressed $MP^{TVCV(K212A/K212A)}$ was infectious. Yet, without directly affecting ER and PD localization, RNA binding, cell-to-cell trafficking, replication, or encapsidation, this NLS mutation reduced TVCV cell-to-cell spread, delayed TVCV systemic spread, and attenuated disease symptoms (Fig. 5 to 8; Tables 1 and 2). Such features typify mutations in viral, bacterial, and fungal proteins that suppress host defenses (53–55).

Pertinent to how nuclear MP^{TVCV} might act as a virulence factor is our demonstration that nuclear MP^{TVCV} localizes to F-actin filaments that appear to associate with discrete regions of chromatin (Fig. 3). Recent studies in yeast, animal cells, and plants point to roles for nuclear actin and actin-related proteins (ARPs) in many aspects of genetic and epigenetic regulation, including transcription, mRNA processing, gene movement, and chromatin remodeling (56, 57). Most of these functions relate to actin-ARP dimers binding to the ATPase subunit of SWI/SNF- and INO80-family chromatin remodeling complexes, where they positively regulate ATPase activity and are essential for remodeler complex assembly to reposition, reconfigure, or eject nucleosomes. As such, they coordinate with histone modifiers (e.g., histone acetyltransferases [HATs]) to recruit DNA-binding proteins to activate or repress transcription or remodel chromosome regions (58–60). The forms of nuclear actin remain enigmatic. In the current view, nuclear actin exists as a dynamic pool of monomeric (G), oligomeric, and polymeric forms. Polymerized nuclear actin has been implicated in selective gene activation during cellular differentiation, the inflammatory response, and retinoic acid-induced transcription (57, 61). Indeed, recent studies using synthetic inducible gene arrays, or of estrogen-induced interactions among genes on different chromosomes, indicate a role for polymerized actin in gene positioning and large-scale chromatin organization (62–64). But, the recent study of *Oct4* reactivation in mouse cell nuclei transplanted into GVs provides the first clear visualization of nuclear F-actin during transcriptional activation and evidence for its role in binding BAF remodeling complexes to enhance transcription (32). We propose that the nuclear function of MP^{TVCV} is to induce or stabilize F-actin filaments to spatially reorganize chromatin and thereby affect the expression of antiviral defense-related host genes.

Our results establish a nuclear function for MP^{TVCV} that is necessary for efficient TVCV cell-to-cell movement and systemic infection and which involves MP^{TVCV} localizing to F-actin filaments that associate with chromatin. Several observations suggest that nuclear localization does not simply serve to downregulate MP^{TVCV} cytoplasmic levels late in infection, either by diverting MP^{TVCV} to the nucleus or by targeting it for degradation: nuclear MP^{TVCV} was present at the earliest stages of and throughout infection, infection with the NLS mutant TVCV::$MP^{K210A/K212A}$ did not affect the distribution and subcellular associations of cytoplasmic MP^{TVCV} (Fig. 3), and MP^{TVCV} was degraded in the absence of nuclear targeting (Fig. 5; the relative sizes of the dark centers in TVCV::$MP^{K210A/K212A}$ versus wt TVCV infection rings were unchanged). Based on the roles of nuclear actin and ARPs in structurally organizing chromatin and regulating gene transcription (62–64), we propose that MP^{TVCV}-containing F-actin nuclear filaments associate with actin and/or ARPs in chromatin remodeling complexes to spatially organize chromatin and thereby coordinately reprogram the transcription of host genes to favor virus infection. Whether the transcription of host defense-related genes, as we propose, or that of host genes that generally affect cellular metabolism and function is altered is now an important question to be answered.

ACKNOWLEDGMENTS

We thank Asako Uchiyama, Greg Ray, and Parth Jarvia in our lab for rousing discussions and helpful suggestions. We also thank Asako Uchiyama for providing pSITE2NB::MP^{TVCV}-GFP and pSITE4NB::MP^{TVCV}-RFP; Greg Ray for help with protoplast isolation; Michael Goodin (University of Kentucky, KY, USA) for pSITE vectors and for the histone 2B-RFP-, fibrillarin-RFP-, and talin-GFP-expressing *N. benthamiana* lines; Karl Oparka (University of Edinburgh, Edinburgh, United Kingdom) for the TMV::MP-GFP infectious clone and *N. benthamiana* plants expressing TUA-GFP; Shoko Ueki and Vitaly Citovsky (SUNY Stony Brook) for pBluescript KS(+)-TVCV-MP and pTVCV50; and Jeffrey Roberts (Cornell University) for use of his Typhoon system.

This research was supported by Public Health Service grant AI-066054 from the National Institute of Allergy and Infectious Diseases to S.G.L.

REFERENCES

1. **Schoelz JE, Harries PA, Nelson RS.** 2011. Intracellular transport of plant viruses: finding the door out of the cell. Mol. Plant **4**:813–831.
2. **Lazarowitz SG, Beachy RN.** 1999. Viral movement proteins as probes for intracellular and intercellular trafficking in plants. Plant Cell **11**:535–548.
3. **Verchot-Lubicz J, Torrance L, Solovyev AG, Morozov SY, Jackson AO, Gilmer D.** 2010. Varied movement strategies employed by triple gene block-encoding viruses. Mol. Plant Microbe Interact. **23**:1231–1247.
4. **Lazarowitz SG.** 2001. The plant viruses, p 533–598. *In* Knipe DM, Howley PM, Griffin DE, Lamb RA, Martin MA, Roizman B, Straus SE (ed), Fields virology, 4th ed. Lippincott Williams & Wilkins, Philadelphia, PA.
5. **Waigmann E, Lucas WJ, Citovsky V, Zambryski P.** 1994. Direct functional assay for tobacco mosaic virus cell-to-cell movement protein and identification of a domain involved in increasing plasmodesmal permeability. Proc. Natl. Acad. Sci. U. S. A. **91**:1433–1437.
6. **Heinlein M, Padgett HS, Gens JS, Pickard BG, Casper SJ, Epel BL, Beachy RN.** 1998. Changing patterns of localization of the tobacco mosaic virus movement protein and replicase to the endoplasmic reticulum and microtubules during infection. Plant Cell **10**:1107–1120.
7. **Mas P, Beachy RN.** 1999. Replication of tobacco mosaic virus on endoplasmic reticulum and role of the cytoskeleton and virus movement protein in intracellular distribution of viral RNA. J. Cell Biol. **147**:945–958.
8. **Asurmendi S, Berg RH, Koo JC, Beachy RN.** 2004. Coat protein regulates formation of replication complexes during tobacco mosaic virus infection. Proc. Natl. Acad. Sci. U. S. A. **101**:1415–1420.
9. **Curin M, Ojangu EL, Trutnyeva K, Ilau B, Truve E, Waigmann E.** 2007. MPB2C, a microtubule-associated plant factor, is required for microtubular accumulation of tobacco mosaic virus movement protein in plants. Plant Physiol. **143**:801–811.
10. **Kragler F, Curin M, Trutnyeva K, Gansch A, Waigmann E.** 2003. MPB2C, a microtubule-associated plant protein binds to and interferes with cell-to-cell transport of tobacco mosaic virus movement protein. Plant Physiol. **132**:1870–1883.
11. **Reichel C, Beachy RN.** 2000. Degradation of tobacco mosaic virus movement protein by the 26S proteasome. J. Virol. **74**:3330–3337.
12. **Wright KM, Wood NT, Roberts AG, Chapman S, Boevink P, Mackenzie KM, Oparka KJ.** 2007. Targeting of TMV movement protein to plasmodesmata requires the actin/ER network: evidence from FRAP. Traffic **8**:21–31.
13. **Aguilar I, Sanchez F, Martin AM, Martinez-Herrera D, Ponz F.** 1996. Nucleotide sequence of Chinese rape mosaic virus (oilseed rape mosaic virus), a crucifer tobamovirus infectious on *Arabidopsis thaliana*. Plant Mol. Biol. **30**:191–197.
14. **Lartey RT, Voss TC, Melcher U.** 1996. Tobamovirus evolution: gene overlaps, recombination, and taxonomic implications. Mol. Biol. Evol. **13**:1327–1338.
15. **Chakrabarty R, Banerjee R, Chung SM, Farman M, Citovsky V, Hogenhout SA, Tzfira T, Goodin M.** 2007. pSITE vectors for stable integration or transient expression of autofluorescent protein fusions in plants: probing *Nicotiana benthamiana*-virus interactions. Mol. Plant Microbe Interact. **20**:740–750.
16. **Zhang Y, Lartey RT, Hartson SD, Voss TC, Melcher U.** 1999. Limita-

tions to tobacco mosaic virus infection of turnip. Arch. Virol. **144**:957–971.
17. **Weiner MP, Costa GL, Schoettlin W, Cline J, Mathur E, Bauer JC.** 1994. Site-directed mutagenesis of double-stranded DNA by the polymerase chain reaction. Gene **151**:119–123.
18. **Burkel BM, von Dassow G, Bement WM.** 2007. Versatile fluorescent probes for actin filaments based on the actin-binding domain of utrophin. Cell Motil. Cytoskeleton **64**:822–832.
19. **Martin K, Kopperud K, Chakrabarty R, Banerjee R, Brooks R, Goodin MM.** 2009. Transient expression in *Nicotiana benthamiana* fluorescent marker lines provides enhanced definition of protein localization, movement and interactions *in planta*. Plant J. **59**:150–162.
20. **Levy A, Erlanger M, Rosenthal M, Epel BL.** 2007. A plasmodesmata-associated beta-1,3-glucanase in Arabidopsis. Plant J. **49**:669–682.
21. **Lewis JD, Lazarowitz SG.** 2010. Arabidopsis synaptotagmin SYTA regulates endocytosis and virus movement protein cell-to-cell transport. Proc. Natl. Acad. Sci. U. S. A. **107**:2491–2496.
22. **Haseloff J, Siemering KR, Prasher DC, Hodge S.** 1997. Removal of a cryptic intron and subcellular localization of green fluorescent protein are required to mark transgenic Arabidopsis plants brightly. Proc. Natl. Acad. Sci. U. S. A. **94**:2122–2127.
23. **Gillespie T, Boevink P, Haupt S, Roberts AG, Toth R, Valentine T, Chapman S, Oparka KJ.** 2002. Functional analysis of a DNA-shuffled movement protein reveals that microtubules are dispensable for the cell-to-cell movement of tobacco mosaic virus. Plant Cell **14**:1207–1222.
24. **Lartey R, Ghoshroy S, Ho J, Citovsky V.** 1997. Movement and subcellular localization of a tobamovirus in Arabidopsis. Plant J. **12**:537–545.
25. **Pascal E, Sanderfoot AA, Ward BM, Medville R, Turgeon R, Lazarowitz SG.** 1994. The geminivirus BR1 movement protein binds single-stranded DNA and localizes to the cell nucleus. Plant Cell **6**:995–1006.
26. **Szecsi J, Ding XS, Lim CO, Bendahmane M, Cho MJ, Nelson RS, Beachy RN.** 1999. Development of tobacco mosaic virus infection sites in *Nicotiana benthamiana*. Mol. Plant Microbe Interact. **12**:143–152.
27. **Oparka KJ, Prior DA, Santa Cruz S, Padgett HS, Beachy RN.** 1997. Gating of epidermal plasmodesmata is restricted to the leading edge of expanding infection sites of tobacco mosaic virus (TMV). Plant J. **12**:781–789.
28. **Beachy RN, Heinlein M.** 2000. Role of P30 in replication and spread of TMV. Traffic **1**:540–544.
29. **Harries PA, Schoelz JE, Nelson RS.** 2010. Intracellular transport of viruses and their components: utilizing the cytoskeleton and membrane highways. Mol. Plant Microbe Interact. **23**:1381–1393.
30. **Frederick RD, Thilmony RL, Sessa G, Martin GB.** 1998. Recognition specificity for the bacterial avirulence protein AvrPto is determined by Thr-204 in the activation loop of the tomato Pto kinase. Mol. Cell **2**:241–245.
31. **Kotlizky G, Katz A, vander Laak J, Boyko V, Lapidot M, Beachy RN, Heinlein M, Epel BL.** 2001. A dysfunctional movement protein of tobacco mosaic virus interferes with targeting of wild-type movement protein to microtubules. Mol. Plant Microbe Interact. **14**:895–904.
32. **Miyamoto K, Pasque V, Jullien J, Gurdon JB.** 2011. Nuclear actin polymerization is required for transcriptional reprogramming of Oct4 by oocytes. Genes Dev. **25**:946–958.
33. **Citovsky V, Wong ML, Shaw AL, Prasad BV, Zambryski P.** 1992. Visualization and characterization of tobacco mosaic virus movement protein binding to single-stranded nucleic acids. Plant Cell **4**:397–411.
34. **Deom CM, Oliver MJ, Beachy RN.** 1987. The 30-kilodalton gene product of tobacco mosaic virus potentiates virus movement. Science **237**:389–394.
35. **Harries P, Ding BA.** 2011. Cellular factors in plant virus movement: at the leading edge of macromolecular trafficking in plants. Virology **411**:237–243.
36. **McLean BG, Zupan J, Zambryski PC.** 1995. Tobacco mosaic virus movement protein associates with the cytoskeleton in tobacco cells. Plant Cell **7**:2101–2114.
37. **Harries PA, Park JW, Sasaki N, Ballard KD, Maule AJ, Nelson RS.** 2009. Differing requirements for actin and myosin by plant viruses for sustained intercellular movement. Proc. Natl. Acad. Sci. U. S. A. **106**:17594–17599.
38. **Kawakami S, Watanabe Y, Beachy RN.** 2004. Tobacco mosaic virus infection spreads cell to cell as intact replication complexes. Proc. Natl. Acad. Sci. U. S. A. **101**:6291–6296.
39. **Liu JZ, Blancaflor EB, Nelson RS.** 2005. The tobacco mosaic virus 126-kilodalton protein, a constituent of the virus replication complex, alone or within the complex aligns with and traffics along microfilaments. Plant Physiol. **138**:1853–1865.
40. **Nejidat A, Cellier F, Holt CA, Gafny R, Eggenberger AL, Beachy RN.** 1991. Transfer of the movement protein gene between two tobamoviruses: influence on local lesion development. Virology **180**:318–326.
41. **Solis I, Garcia-Arenal F.** 1990. The complete nucleotide sequence of the genomic RNA of the tobamovirus tobacco mild green mosaic virus. Virology **177**:553–558.
42. **Morishima N, Ido T, Hamada H, Yoshimoto E, Mizumoto H, Takeuchi S, Kiba A, Hikichi Y, Okuno T.** 2003. Infectious in vitro transcripts from a cDNA clone of *Tobacco mild green mosaic tobamovirus* and its biological activity in host and nonhost plants and in their protoplasts. J. Gen. Plant Pathol. **69**:335–338.
43. **Fenczik CA, Padgett HS, Holt CA, Casper SJ, Beachy RN.** 1995. Mutational analysis of the movement protein of odontoglossum ringspot virus to identify a host-range determinant. Mol. Plant Microbe Interact. **8**:666–673.
44. **Ingham DJ, Pascal E, Lazarowitz SG.** 1995. Both bipartite geminivirus movement proteins define viral host range, but only BL1 determines viral pathogenicity. Virology **207**:191–204.
45. **Renovell A, Carmen Vives M, Ruiz-Ruiz S, Navarro L, Moreno P, Guerri J.** 2012. The citrus leaf blotch virus movement protein acts as silencing suppressor. Virus Genes **44**:131–140.
46. **Weber H, Ohnesorge S, Silber MV, Pfitzner AJ.** 2004. The tomato mosaic virus 30 kDa movement protein interacts differentially with the resistance genes Tm-2 and Tm-2(2). Arch. Virol. **149**:1499–1514.
47. **Matsushita Y, Deguchi M, Youda M, Nishiguchi M, Nyunoya H.** 2001. The tomato mosaic tobamovirus movement protein interacts with a putative transcriptional coactivator KELP. Mol. Cells **12**:57–66.
48. **Matsushita Y, Miyakawa O, Deguchi M, Nishiguchi M, Nyunoya H.** 2002. Cloning of a tobacco cDNA coding for a putative transcriptional coactivator MBF1 that interacts with the tomato mosaic virus movement protein. J. Exp. Bot. **53**:1531–1532.
49. **Fontes EP, Santos AA, Luz DF, Waclawovsky AJ, Chory J.** 2004. The geminivirus nuclear shuttle protein is a virulence factor that suppresses transmembrane receptor kinase activity. Genes Dev. **18**:2545–2556.
50. **Santos AA, Lopes KV, Apfata JA, Fontes EP.** 2010. NSP-interacting kinase, NIK: a transducer of plant defence signalling. J. Exp. Bot. **61**:3839–3845.
51. **Carvalho MF, Lazarowitz SG.** 2004. Interaction of the movement protein NSP and the Arabidopsis acetyltransferase AtNSI is necessary for cabbage leaf curl geminivirus infection and pathogenicity. J. Virol. **78**:11161–11171.
52. **Carvalho MF, Turgeon R, Lazarowitz SG.** 2006. The geminivirus nuclear shuttle protein NSP inhibits the activity of AtNSI, a vascular-expressed Arabidopsis acetyltransferase regulated with the sink-to-source transition. Plant Physiol. **140**:1317–1330.
53. **Aliyari R, Ding SW.** 2009. RNA-based viral immunity initiated by the Dicer family of host immune receptors. Immunol. Rev. **227**:176–188.
54. **Bierne H, Cossart P.** 2012. When bacteria target the nucleus: the emerging family of nucleomodulins. Cell. Microbiol. **14**:622–633.
55. **Cui J, Shao F.** 2011. Biochemistry and cell signaling taught by bacterial effectors. Trends Biochem. Sci. **36**:532–540.
56. **Meagher RB, Kandasamy MK, Smith AP, McKinney EC.** 2010. Nuclear actin-related proteins at the core of epigenetic control. Plant Signal. Behav. **5**:518–522.
57. **Visa N, Percipalle P.** 2010. Nuclear functions of actin. Cold Spring Harbor Perspect. Biol. **2**:a000620. doi:10.1101/cshperspect.a000620.
58. **Bao Y, Shen X.** 2011. SnapShot: chromatin remodeling: INO80 and SWR1. Cell **144**:158–158.e2. doi:10.1016/j.cell.2010.12.024.
59. **Cairns BR.** 2009. The logic of chromatin architecture and remodelling at promoters. Nature **461**:193–198.
60. **Kasten MM, Clapier CR, Cairns BR.** 2011. SnapShot: chromatin remodeling: SWI/SNF. Cell **144**:310.e311. doi:10.1016/j.cell.2011.01.007.
61. **Miyamoto K, Gurdon JB.** 2011. Nuclear actin and transcriptional activation. Commun. Integr. Biol. **4**:582–583.
62. **Chuang CH, Carpenter AE, Fuchsova B, Johnson T, de Lanerolle P, Belmont AS.** 2006. Long-range directional movement of an interphase chromosome site. Curr. Biol. **16**:825–831.
63. **Dundr M, Ospina JK, Sung MH, John S, Upender M, Ried T, Hager GL, Matera AG.** 2007. Actin-dependent intranuclear repositioning of an active gene locus in vivo. J. Cell Biol. **179**:1095–1103.
64. **Hu Q, Kwon YS, Nunez E, Cardamone MD, Hutt KR, Ohgi KA, Garcia-Bassets I, Rose DW, Glass CK, Rosenfeld MG, Fu XD.** 2008. Enhancing nuclear receptor-induced transcription requires nuclear motor and LSD1-dependent gene networking in interchromatin granules. Proc. Natl. Acad. Sci. U. S. A. **105**:19199–19204.